

Properties of magnesium alloys reinforced with nanoparticles and carbon nanotubes: a review

Hajo Dieringa

Received: 26 August 2010 / Accepted: 14 October 2010 / Published online: 30 October 2010
© Springer Science+Business Media, LLC 2010

Abstract Magnesium alloys suffer from only moderate high-temperature strength and creep resistance. Aluminium-free magnesium alloys for sand casting or alloys containing aluminium with expensive additional alloying elements may be in use, but only microparticle or microfibre-reinforced magnesium alloys really exhibit satisfactory creep strengths at temperatures up to 250 °C. Reinforcing magnesium alloys with ceramic nanoparticles could be a solution for preserving a low density while increasing the high-temperature performance. When produced using melting processes, nanoparticle-reinforced magnesium composites are expected to enjoy strengthening due to the grain refinement described in the Hall–Petch relation. When an isotropic distribution of nanoparticles is achieved, the composites are additionally expected to be Orowan-strengthened. In this review, a variety of ceramic materials, such as SiC, Al₂O₃, Y₂O₃, SiO₂ and carbon nanotubes were investigated for reinforcement. Pure magnesium and various magnesium alloys were chosen as the matrix material and both powder metallurgical (PM) and melting processes were used for production of the composites. The mechanical properties of the composites were generally enhanced, compared to an unreinforced alloy; not only at room temperature, but also at elevated temperatures. In some cases an increase in strength in combination with increased ductility was also identified.

Introduction

During the last two decades, automotive engineers have increasingly focused on magnesium alloys due to their low density and their resulting high specific strengths. In the earlier part of the last century, magnesium alloys suffered from low corrosion resistance, usually due to iron, copper and nickel impurities, but nowadays alloys with good corrosion properties and coatings are available. High-pressure die casting is the process used for approximately 90% of magnesium alloys, and most of it is produced for room temperature applications. Aluminium–zinc (AZ91, AZ60) and aluminium–manganese (AM50, AM60) magnesium alloys are widely used for this purpose, not only in the automotive but also electronic and machine-tool applications. These alloys exhibit good room-temperature strength, corrosion resistance, and are able to be cast and machined. During solidification the magnesium aluminium β -phase Mg₁₇Al₁₂ forms, which is known to weaken at higher temperatures [1]. When it comes to utilisation at higher temperatures, such as in gearbox housings, more sophisticated alloys are used. Often aluminium-free alloys are used to avoid the β -phase, but when aluminium is used, because it improves castability, additional alloying elements are chosen that form precipitates during solidification and are favourable compared to magnesium, in order to avoid the formation of Mg₁₇Al₁₂ and also to enhance the material by precipitation strengthening. Calcium, rare earth elements, strontium and silicon are all elements used for high-temperature alloys. However, strengthening for temperature regions above 175 °C is difficult. Only some sand cast alloys containing silver with rare earth elements (QE22) and yttrium with rare earth elements (WE43, WE54) give good creep resistance in these temperature regions. Magnesium-based metal matrix composites reinforced with ceramic

H. Dieringa (✉)
Helmholtz-Zentrum Geesthacht,
Centre for Materials and Coastal Research,
Max-Planck-Str. 1, 21502 Geesthacht, Germany
e-mail: hajo.dieringa@hzg.de

fibres and/or particles in micrometer scale have proven outstanding creep and wear resistance, and provide strength even at high temperatures. Their disadvantages are the high production cost and their poor machinability. Since ceramic nanoparticles and fibres are widely available and are inexpensive, these reinforcements are used for strengthening magnesium alloys. Not only are the mechanical properties improved by the particle strengthening effect (Orowan strengthening) but also by the grain refining effect during solidification.

Orowan strengthening does not play a fundamental role in microparticle-reinforced MMC, because of the inter-particle spacing and the particles are too large [2]. Besides effects such as the generation of dislocations due to thermal mismatch between ceramic particles and the metallic matrix, which strengthen the material or load bearing of the reinforcement, the pure Orowan strengthening effect can be described by the Orowan–Eshby Eq. 1:

$$\Delta\sigma_{\text{Oro}} = \frac{0.13G_m b}{\lambda} \ln \frac{r}{b} \quad (1)$$

where $\Delta\sigma_{\text{Oro}}$ is the increase in yield strength by Orowan strengthening, G_m the shear modulus of the matrix, b the Burgers vector, λ the inter-particle spacing and r the particle radius. Usually λ can be estimated as follows:

$$\lambda \approx d_p \left[\left(\frac{1}{2V_p} \right)^{1/3} - 1 \right] \quad (2)$$

where V_p is the volume fraction of reinforcement [3].

The strengthening effect of grain refinement is described by the Hall–Petch Eq. 3, where σ_y is the yield strength, σ_i the lattice friction, k_y is a material dependent constant and d_g the grain diameter. The lattice friction σ_i can be subdivided into temperature dependent and temperature independent parts. The temperature-dependent Peierls–Nabarro force is related to obstacles with short-range stress fields. The independent part arises from obstacles with long-range stress fields. The interpretation of k_y is less clear. An interpretation is given in [4]

$$\sigma_y = \sigma_i + k_y d_g^{-1/2} \quad (3)$$

In this review, the state of the art in the nanoparticle and nanofibre reinforcement of magnesium alloys is described. The paper is subdivided into the type and structure of ceramic reinforcement.

SiC

In [5], the composite is prepared with a powder metallurgical (PM) method. 3 vol.% SiC particles with a mean diameter of 30 nm and pure magnesium powder with a

mean diameter of 40 μm were mixed for 8 h and milled. After encapsulating and degassing, the material was extruded at 350 $^{\circ}\text{C}$. For the purposes of comparison, pure magnesium powder was treated in the same way. Light optical microscopy showed that a mean grain size of 20 μm was obtained in the pure magnesium and mixed specimens, whereas the mixed and milled specimens exhibited a grain size close to 1 μm . In TEM studies, the SiC nanoparticles were found close to the grain boundaries, forming a network. Tensile tests at RT, 100, 200 and 300 $^{\circ}\text{C}$ showed that the milled composite always exhibits the highest ultimate tensile stress. The smaller grain size, according to the Hall–Petch relationship, is assumed to be responsible for this. Tensile creep tests were performed at 200 $^{\circ}\text{C}$ and with stresses of 35 and 45 MPa. The minimum creep rates are plotted in Fig. 1 and it can be seen that after milling the composite shows the best creep resistance, even if the grain size is smaller compared to the others, which should enhance grain boundary sliding. SiC particles are potentially responsible for hindering this. Estimation of the stress exponent n , as a part of the power-law equation, results in values of ~ 10 and ~ 3 , at temperatures of 200 and 300 $^{\circ}\text{C}$, respectively. A dislocation movement-controlled deformation rather than diffusion creep is assumed to be the dominant process. Reducing the surface roughness of the creep specimens also significantly improves their creep resistance. Comparing the creep results with those of creep-resistant magnesium alloys (WE43, WE54 and QE22) shows that even a small amount of nano-SiC leads to similar or even better creep resistance.

SiC particles with a mean diameter of 0.6 μm and Ti particles with a mean size of 20 μm were used as reinforcement of pure magnesium in [6]. The pure magnesium and two composite materials with different amounts of SiC were produced by disintegrated melt deposition (DMD)

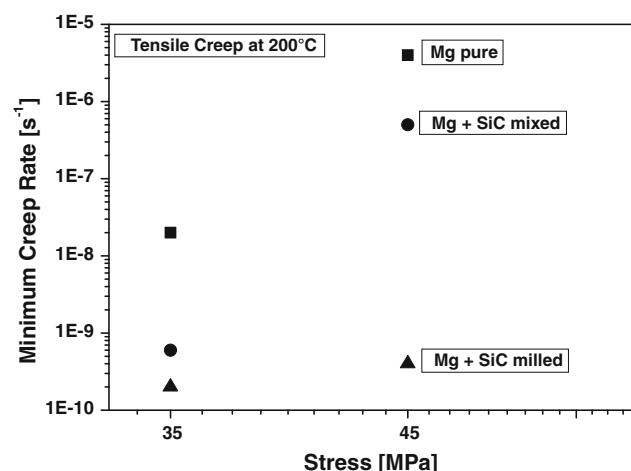


Fig. 1 Minimum creep rates of creep tests performed at 200 $^{\circ}\text{C}$ and 35 and 45 MPa, respectively (according to [5])

and subsequently extruded. The composition of the materials, grain size, coefficient of thermal expansion (CTE) and hardness are given in Table 1.

There is a significant reduction in CTE, together with an increase in hardness, for the composite with 15 wt% SiC. Table 2 shows that with an increasing amount of reinforcement the dynamic modulus increases. By increasing the 0.2 yield strength, the ductility decreases. Micrographs of fracture surfaces show that the titanium particles fractured, which indicates a good bonding between the particles and the magnesium matrix.

The effect of different sizes of SiC reinforcement was studied in [7]. Pure magnesium was reinforced with SiC particles of two different mean diameters, 25 μm and 50 nm, respectively. Mixtures of the powders were compacted to billets and subsequently sintered in a microwave-assisted process. For the purposes of comparison, pure magnesium was treated in the same way. All the billets were subsequently hot extruded. The physical and mechanical properties were examined from a composite with 1 vol.% nm-SiC, a composite with 10 vol.% μm-SiC and a composite with a mixture of both. The results were compared with the pure magnesium sample’s properties. In Table 3, the composition, CTE, materials porosity and the microhardness is given. The hardness increases with an increasing amount of SiC and the CTE is reduced.

A significant increase in UTS and 0.2 YS is reached with a reinforcement of only 1 vol.% nm-SiC and, surprisingly, the ductility is also increased. Composites with 9 or 10 vol.% of μm-SiC and the nm-SiC reinforced composite show an excellent improvement compared to the pure magnesium samples (Table 4).

The microstructure and hardness of nanoparticle-reinforced AZ91 was investigated in [8]. SiC particles with an average diameter of 30 nm were introduced, using a high-intensity ultrasonic wave technique (HEUWT). Two compositions were produced, with 2.0 wt% and 5.0 wt% SiC, respectively. It could be shown that HEUWT is capable of distributing and uniformly dispersing SiC nanoparticles in a magnesium melt. EDS analysis showed that the SiC particles are partly oxidised and that Mg₂Si is formed in the composite. The microhardness increased with an increasing amount of nano-SiC and reached an improvement of 75% with 5 vol.% SiC compared to the pure AZ91.

Again, an ultrasonic process was used in [9] to produce a composite material with SiC particles of 50 nm in diameter. As base alloys, AS21 and AS41 were used, which were mixed from pure elements (without any Mn). An ultrasonic probe was dipped in the molten alloy and, with a power level of 3.5 kW, the added SiC particles were distributed. Feeding the melt with 2 wt% SiC needed

Table 1 Composition, grain size, CTE and hardness of pure Mg and the two composites [6]

Material	wt% reinforcement		Grain size (μm)	CTE (10 ⁻⁶ K ⁻¹)	Macrohardness (HR15T)	Microhardness (HV)
	SiC	Ti				
Mg	–	–	21 ± 6	28.0	47 ± 1	41 ± 1
Mg/SiC/Ti	5.02	2.7	20 ± 6	23.4	48 ± 2	48 ± 1
Mg/SiC/Ti	14.93	2.7	15 ± 4	19.9	65 ± 1	66 ± 1

Table 2 Mechanical properties of pure Mg and the two composites [6]

Material	Dynamic modulus (GPa)	0.2 YS (MPa)	UTS (MPa)	Elongation (%)
Mg	39.8	153 ± 8	207 ± 4	9.2 ± 1.4
Mg/5SiC/2.7Ti	46.8	169 ± 8	204 ± 17	2.7 ± 0.7
Mg/15SiC/2.7Ti	51.8	217 ± 2	233 ± 6	1 ± 0.05

Table 3 SiC content, CTE, porosity and microhardness of pure magnesium and SiC composites [7]

Material	SiC content (vol.%)		CTE (10 ⁻⁶ K ⁻¹)	Porosity (%)	Microhardness (HV)
	25 μm	50 nm			
Pure Mg	–	–	29.1 ± 1.2	0.52	38.6 ± 1.5
Mg + 1% nm-SiC	–	1.0	28.1 ± 0.9	0.11	43.2 ± 2.0
Mg + 10% μm-SiC	10.0	–	25.6 ± 1.9	1.22	44.3 ± 0.5
Hybrid Mg	9.0	1.0	24.9 ± 0.5	1.75	50.9 ± 1.0

Table 4 Mechanical properties of pure magnesium and SiC composites [7]

Material	0.2 YS (MPa)	UTS (MPa)	Elongation (%)
Pure Mg	125 ± 15	172 ± 12	5.8 ± 0.9
Mg + 1% nm-SiC	157 ± 22	203 ± 22	7.6 ± 1.5
Mg + 10% μm-SiC	140 ± 2	165 ± 2	1.5 ± 0.8
Hybrid Mg	156 ± 7	185 ± 11	0.6 ± 0.1

Table 5 Mechanical properties of the alloys and composites with 2 vol.% SiC [9]

Material	YS (MPa)	UTS (MPa)	Elongation (%)
AS21	48.6	137.9	9.2
AS21 + 2SiC	73.8	157.2	7.5
AS41	61.9	144.8	8.8
AS41 + 2SiC	82.1	177.9	9.5

30–40 min and then the process was continued for an additional 15 min. The melt was cast in a permanent mould for producing tensile specimens. Tensile tests show the results listed in Table 5. Yield strength and ultimate tensile strength was significantly increased, while ductility remained good or was even improved, which is in contrast to the μm-reinforced magnesium based MMC. Microstructural investigations show that micro-clusters of SiC particles remained in the material. The grain size was refined by nanosized SiC additions in both alloys, which gives an additional strengthening effect. Process parameters need further optimization in order to get rid of the remaining nanoparticle clusters, occurring mainly at the grain boundaries. Particles not belonging to the clusters were dispersed very well. This seems to be the main reason for the improvement of the mechanical properties, besides grain refinement. SEM images show that nanoparticles at the grain boundaries could be sintered. The still high ductility of the composite materials is attributed to magnesium separation of most of the particles in the clusters and the grain refining and strengthening effects of the well-dispersed particles. In addition, it was found that all the silicon in the matrix alloy reacts with magnesium to Mg₂Si and that the well-bonded SiC nanoparticles have a random orientation in the matrix.

In [10], the fabrication process of nanoparticle-reinforced magnesium alloys is investigated, in terms of simulating the acoustic cavitations and acoustic streaming in magnesium melts. Since it is difficult to observe these effects directly in metallic melts, other liquids were used. Experiments were done in water, glycerol, soybean oil and an oil–water mixture. Acoustic cavitations were tested with aluminium foils in water and it was found that the greater the distance, the lower the impact on the foil. By keeping

the distance constant with increasing frequency, the acoustic cavitations are stronger and by keeping the frequency constant the acoustic cavitations increase with increasing ultrasonic power. The depth of the waveguide tip in the metallic melt is therefore an important factor that influences the dispersion of nanoparticles in liquids. Sound pressure gradients are caused when ultrasonic waves are exerted on the melt. This effect leads to a turbulent flow, which is known as acoustic streaming. The acoustic streaming was investigated in soybean oil and in glycerol as well under three different ultrasonic conditions. Processing with 15 kHz and 2.6 kW induces a fluid jet under the tip while 20 kHz and 1.4 kW causes the strongest turbulent flow in the melt. The scrolled acoustic streaming with 20 kHz and 4 kW is formed after 60 s in glycerol. By reducing the power, the acoustic streaming is formed more quickly. Additional oil dispersion tests in water led to the conclusion that the ultrasonic processing of the oil in water is best at 20 kHz and 1.4 kW power output. 0.5% SiC nanoparticles were distributed in an AZ91 melt, taking the investigated process parameter into account. With 20 kHz and 4 kW the nanoparticles cluster seriously, but with a lower power of 1.4 kW they are dispersed very well.

Al₂O₃

Dislocation generation and changes in the microstructure as a consequence of the thermal cycling of nanoparticle-reinforced pure magnesium are investigated in [11]. Powder mixtures of magnesium and 1 vol.% alumina with diameters of 20 μm and 12 nm, respectively, were mixed and milled for 1 h and subsequently hot extruded at 450 °C. Damping measurements were performed on the annealed specimens. Annealing was done at different temperatures after cooling in liquid nitrogen. It was found that in unreinforced pure magnesium there is nearly no dependence of the logarithmic decrement on the annealing temperatures. However, in the composite material this dependence is stronger. The reason seems to be the increase in internal stresses after cooling, due to the differences in the thermal expansions of magnesium and alumina.

Disintegrated melt deposition (DMD) was used to produce an alumina particle-reinforced pure magnesium composite [12]. A reinforcement of 1.1 vol.% alumina particles with a diameter of 50 nm was added to the superheated melt (750 °C) and mixed under an argon atmosphere. After mixing, the melt was released downwards through an orifice, subsequently disintegrated by two jets of argon gas and deposited on a substrate. Pure magnesium was treated in the same way for comparison. The resulting ingots were hot extruded at 250 °C. Optical

investigation of microstructural features shows a significantly reduced grain size of 14 ± 2 in the composite compared to 49 ± 8 in the pure magnesium. The CTE is significantly reduced by the incorporation of 1.1 vol.% alumina particles. By calculation, in accordance with the rule of mixture (ROM), a value of $28.2 \cdot 10^{-6} \text{ K}^{-1}$ would have been expected. The hardness increase is more than 50% in both directions; the transversal and the longitudinal. Table 6 shows these values and Table 7 gives the mechanical properties. The enormous increase in yield strength is attributed to the high number of randomly distributed particles and the reduction in grain size. An increase in ductility of 89% in the composite compared to pure magnesium is again attributed to grain refinement and finely distributed nanoparticles in the matrix. Fractography showed that with the reinforcement of alumina nanoparticles, the fracture behaviour changed from a brittle to mixed-mode fracture in the composite. Non-basal slip systems were activated additionally.

A PM process with a mixing and subsequent compaction was followed by a hybrid microwave-assisted sintering process in [13] to produce a composite with two scales of alumina particles. Magnesium powder with a size of 60–300 μm and alumina powder of 300 and 50 nm sizes were used for the production. The final stage of production was a hot extrusion at 350 °C. Three combinations of alumina particle fractions were investigated, having in common a sum of 5 vol.% reinforcement, as listed in

Table 8. Experimental values lie between those predicted from the ROM, Kerner’s model and Turner’s model. This indicates a good bonding between particles and matrix. The increase in 0.2 YS, compared to the pure magnesium, is attributed to Orowan strengthening, a decrease in grain size and an increase in dislocation density around the particles. In all cases, the ductility decreases with alumina reinforcement (Table 9).

Magnesium powder with a diameter of 30–60 μm and the addition of 2.5 wt% alumina powder with a diameter of 50 nm was mixed, pressed, sintered and hot extruded at 250 °C [14]. Pure magnesium was processed in the same way for comparison. The presence of nanosized alumina reduces the grain size and improves the micro and macro-hardness as shown in Table 10. The mechanical properties significantly increased as well as the ductility in the composite as shown in Table 11. Again, the finer grain size of the recrystallized grains is attributed to the capability of nanosized alumina to nucleate magnesium grains during recrystallization and to restrict the growth of grains by grain-boundary pinning. Once more, the increase in 0.2 YS and UTS is attributed to a smaller grain size in combination with a higher dislocation density in the matrix, due to the thermal mismatch of alumina and magnesium, and a good bonding with a resultant good load transfer at the interface. The surprising increase in ductility is thought to be due to multidirectional thermal stresses at the interface, which starts multi-directional dislocation movement.

Table 6 Grain size, CTE, density and hardness of pure Mg and the composite [12]

Material	Density (g/cm^3)		Grain size (μm)	CTE (10^{-6} K^{-1})	Microhardness (HV)	
	Theor.	Exp.			Transverse	Longitudinal
Mg	1.74	1.7397	49 ± 8	28.4 ± 0.3	39.97 ± 0.22	40.06 ± 0.29
Mg + 1.1Al ₂ O ₃	1.7647	1.7623	14 ± 2	25.1 ± 0.3	65.92 ± 0.86	66.17 ± 0.58

Table 7 Mechanical properties of pure Mg and the composite [12]

Material	<i>E</i> (GPa)	0.2 YS (MPa)	UTS (MPa)	Elongation (%)	$\sigma_{0.2YS}/\rho$	σ_{UTS}/ρ	Work of fracture (J/m^3)
Mg	42.8	97 ± 2	173 ± 1	7.4 ± 0.2	56	99	11.1 ± 0.3
Mg + 1.1Al ₂ O ₃	52.7	175 ± 3	246 ± 3	14 ± 2.4	99	140	31.7 ± 6.3

Table 8 Composition, density, grain size and CTE of pure Mg and investigated composites [13]

Material	Amount of Al ₂ O ₃ (vol.%)		Density (g/cm^3)		Grain size (μm)	CTE (10^{-6} K^{-1})
	50 nm	300 nm	Theor.	Exp.		
Mg	–	–	1.740	1.738 ± 0.001	36 ± 4	28.6 ± 0.8
Mg/Al ₂ O ₃	0.5	4.5	1.851	1.840 ± 0.003	24 ± 8	27.2 ± 1.2
Mg/Al ₂ O ₃	0.75	4.25	1.851	1.837 ± 0.005	27 ± 9	25.7 ± 0.6
Mg/Al ₂ O ₃	1	4	1.851	1.831 ± 0.005	31 ± 7	25.8 ± 0.8

Table 9 Mechanical properties of pure magnesium and investigated composites [13]

Material	Amount of Al ₂ O ₃ (vol.%)		Youngs modulus (GPa)	0.2 YS (MPa)	UTS (MPa)	Elongation (%)
	50 nm	300 nm				
Mg	–	–	45	116 ± 11.1	168 ± 10	9.0 ± 0.3
Mg/Al ₂ O ₃	0.5	4.5	50.5	139 ± 26.5	187 ± 28	1.9 ± 0.2
Mg/Al ₂ O ₃	0.75	4.25	51.9	138 ± 13.2	189 ± 15	2.4 ± 0.6
Mg/Al ₂ O ₃	1	4	54.4	157 ± 20.3	211 ± 21	3.0 ± 0.3

Table 10 Alumina content, density, grain size and hardness of pure Mg and the composite [14]

Material	Alumina (vol.%)	Density (g/cm ³)	Grain size (μm)	Microhardness (HV)	Macrohardness (HR15T)
Mg	–	1.7387 ± 0.0022	60 ± 10	40 ± 0	37 ± 1
Mg2.5Al ₂ O ₃	1.1	1.7632 ± 0.0048	31 ± 13	66 ± 1	65 ± 1

Table 11 Mechanical properties of pure Mg and the composite [14]

Material	<i>E</i> (GPa)	0.2 YS (MPa)	UTS (MPa)	Ductil. (%)	$\sigma_{0.2YS}/\rho$	σ_{UTS}/ρ
Mg	41.2	132 ± 7	193 ± 2	4.22 ± 0.08	76	111
Mg2.5Al ₂ O ₃	44.5	194 ± 5	250 ± 3	6.89 ± 1.01	110	142

Magnesium reinforced with three different amounts of 300 nm alumina particles are investigated in [15]. The material was produced using the DMD process, followed by hot extrusion as described in [12]. Three different amounts of alumina particles were introduced: 1.5, 2.5 and 5.5 wt%. The results of an investigation into the morphology, density and grain size are shown in Table 12. Microstructural investigations have shown that the reinforcement was distributed randomly in the matrix and the magnesium recrystallized completely after extrusion. The finer grain size is again attributed to nucleation of

magnesium grains by alumina particles and the grain growth restriction of the particles during recrystallization (Table 13).

In a further study by the same authors, pure magnesium was reinforced with 2.5 wt% alumina of three different sizes: 50 nm, 300 nm and 1 μm [16]. The materials were produced by mixing the powder, compacting it and subsequently sintering. After hot extrusion at 250 °C, microstructural investigations and mechanical testing was performed. The best 0.2 YS and UTS are found in the composite with 50 nm alumina particles. Ductility

Table 12 Density, porosity and grain size of Mg and the composites [15]

Material	Alumina content (wt%)	Density (g/cm ³)		Porosity (%)	Grain size (μm)
		Theor.	Exp.		
Mg	–	1.7400	1.7397 ± 0.0009	0.02	49 ± 8
Mg0.7Al ₂ O ₃	1.5	1.7548	1.7541 ± 0.0029	0.04	6 ± 2
Mg1.1Al ₂ O ₃	2.5	1.7647	1.7636 ± 0.0013	0.06	6 ± 1
Mg2.5Al ₂ O ₃	5.5	1.7954	1.7897 ± 0.0044	0.32	4 ± 1

Table 13 Mechanical properties of Mg and the composites [15]

Material	0.2 YS (MPa)	UTS (MPa)	Ductility (%)	WF (J/m ³)	$\sigma_{0.2YS}/\rho$	σ_{UTS}/ρ
Mg	97 ± 2	173 ± 1	7.4 ± 0.2	11.1 ± 0.3	56	99
Mg0.7Al ₂ O ₃	214 ± 4	261 ± 5	12.5 ± 1.8	28.9 ± 4.7	122	149
Mg1.1Al ₂ O ₃	200 ± 1	256 ± 1	8.6 ± 1.1	20.9 ± 2.8	113	145
Mg2.5Al ₂ O ₃	222 ± 2	281 ± 5	4.5 ± 0.5	10.0 ± 1.3	124	157

increases with increasing particle size. The work of fracture, which expresses the ability of energy absorption up to the moment of fracture, increases with increasing particle size. It is much higher in each composite compared to pure magnesium. In an additional study, the authors summarised the material properties of nanocomposites produced from powder with a DMD process [17]. The composites produced by DMD show a more uniform particle distribution and a finer grain size, compared to PM processing. The dimensional stability, in terms of CTE, is much better in a DMD processed composite, whereas the mechanical properties are comparable in both cases. Composites with different sizes of particles were also produced using the

DMD technique [18]. It enables a direct comparison between the materials processed in two different ways (Tables 14, 15, 16, 17).

The same authors have also compared nanocomposites produced using the blend-press-sinter PM process [19]. The process is already described and the results of mechanical testing and microstructural characterisation are given in Tables 18 and 19.

For evaluating the damping behaviour of alumina nanoparticles-reinforced pure magnesium a PM method was chosen to produce the composite [20]. Magnesium powder with a diameter of 60–300 μm was blended with 1 wt% (= 0.4 vol.%) alumina powder with an average

Table 14 Density, porosity, grain size and inter-particle spacing of all materials [16]

Material	Density (g/cm ³)		Porosity (%)	Grain size (μm)	Interparticle spacing λ (μm)
	Theor.	Exp.			
Mg	1.7400	1.7378 ± 0.0022	0.08	60 ± 10	–
Mg/Al ₂ O ₃ (50 nm)	1.7647	1.7632 ± 0.0048	0.09	31 ± 13	0.47
Mg/Al ₂ O ₃ (300 nm)	1.7647	1.7646 ± 0.0009	0.01	11 ± 4	2.85
Mg/Al ₂ O ₃ (1 μm)	1.7647	1.7645 ± 0.0013	0.01	11 ± 3	9.49

Table 15 Mechanical properties of Mg and the composites [16]

Material	Hardness		0.2 YS (MPa)	UTS (MPa)	Ductility (%)	Work of fracture (J/m ³)
	Macro (15 HRT)	Micro (HV)				
Mg	43.5 ± 0.3	37.4 ± 0.4	132 ± 7	193 ± 2	4.2 ± 0.1	7.1 ± 0.3
Mg/Al ₂ O ₃ (50 nm)	59.7 ± 0.5	69.5 ± 0.5	194 ± 5	250 ± 3	6.9 ± 1.0	15.5 ± 2.6
Mg/Al ₂ O ₃ (300 nm)	56.3 ± 0.5	51.8 ± 0.3	182 ± 3	237 ± 1	12.1 ± 1.4	25.0 ± 3.3
Mg/Al ₂ O ₃ (1 μm)	50.3 ± 0.5	51.2 ± 0.5	172 ± 1	227 ± 2	16.8 ± 0.4	34.7 ± 0.8

Table 16 Density, porosity and grain size of Mg and the composites [18]

Material	Density (g/cm ³)		Porosity (%)	Grain size (μm)
	Theor.	Exp.		
Mg	1.7400	1.7397 ± 0.0009	0.02	49 ± 8
Mg/Al ₂ O ₃ (50 nm)	1.7647	1.7623 ± 0.0019	0.07	14 ± 2
Mg/Al ₂ O ₃ (300 nm)	1.7647	1.7636 ± 0.0013	0.06	6 ± 1
Mg/Al ₂ O ₃ (1 μm)	1.7647	1.7614 ± 0.0068	0.19	5 ± 1

Table 17 Mechanical properties of Mg and the composites [18]

Material	Hardness		0.2 YS (MPa)	UTS (MPa)	Ductility (%)	Work of fracture (J/m ³)
	Macro (15 HRT)	Micro (HV)				
Mg	37.1 ± 0.7	40.0 ± 0.2	97 ± 2	173 ± 1	7.4 ± 0.2	11.1 ± 0.3
Mg/Al ₂ O ₃ (50 nm)	64.6 ± 0.8	65.9 ± 0.9	175 ± 3	246 ± 3	14.0 ± 2.4	31.7 ± 6.3
Mg/Al ₂ O ₃ (300 nm)	59.4 ± 0.6	52.0 ± 0.8	200 ± 1	256 ± 1	8.6 ± 1.1	20.9 ± 2.8
Mg/Al ₂ O ₃ (1 μm)	63.8 ± 0.5	58.8 ± 0.5	209 ± 1	242 ± 3	3.5 ± 0.3	7.0 ± 0.9

Table 18 Density, porosity and grain size of Mg and the composites [19]

Material	Alumina content (wt%)	Density (g/cm ³)		Porosity (%)	Grain size (μm)
		Theor.	Exp.		
Mg	–	1.7400	1.7387 ± 0.0022	0.08	60 ± 10
Mg0.22Al ₂ O ₃	0.5	1.7449	1.7421 ± 0.0078	0.16	61 ± 18
Mg0.66Al ₂ O ₃	1.5	1.7548	1.7501 ± 0.0026	0.27	63 ± 16
Mg1.11Al ₂ O ₃	2.5	1.7647	1.7632 ± 0.0048	0.09	31 ± 13

Table 19 Mechanical properties of Mg and the composites [19]

Material	Hardness		<i>E</i> (GPa)	0.2 YS (MPa)	UTS (MPa)	Ductility (%)	Work of fracture (J/m ³)
	Macro (15 HRT)	Micro (HV)					
Mg	43 ± 0	37 ± 0	41.2	132 ± 7	193 ± 2	4.2 ± 0.1	7.1 ± 0.3
Mg0.22Al ₂ O ₃	51 ± 0	44 ± 0	42.5	169 ± 4	232 ± 4	6.5 ± 2.0	13.5 ± 4.5
Mg0.66Al ₂ O ₃	56 ± 0	50 ± 1	43.4	191 ± 2	247 ± 2	8.8 ± 1.6	19.9 ± 3.9
Mg1.11Al ₂ O ₃	60 ± 1	70 ± 0	44.5	194 ± 5	250 ± 3	6.9 ± 1.0	15.5 ± 2.6

diameter of 50 nm. After cold compaction, the ingots were hot extruded at 400 °C. Some properties are listed in Table 20. Damping was measured with ‘Free–Free’ or ‘Suspended’ beam methods in accordance with the ASTM C1259-98 standard. The experimental damping loss factor of pure magnesium was found to be 0.0085. Having an average particle size of 50 nm and being randomly distributed in the magnesium matrix, an inter-particle spacing of 0.75 μm can be assumed. The loss factor of pure alumina is 0.0009, but the composite material shows an experimental loss factor of 0.0115. The higher loss factor is the reason for the faster settling of the vibration amplitude with time, compared to the unreinforced magnesium. The higher value is assumed to be a result of the existence of a

plastic zone, due to the high differences in CTE as well as due to an increase in dislocation density around the particles.

Different amounts of 50 nm alumina powder were introduced into pure magnesium powder and subsequently extruded [21]. 1, 3 and 5 wt% were blended with the magnesium powder (60–300 μm), cold compacted and extruded at 200 °C. In addition, the influence of extrusion temperature and sintering was investigated, when the same material was sintered for 1 h at 500 °C and hot extruded at 400 °C. Microstructural investigations revealed a uniform distribution of alumina particles in all the materials. First, the thermal and mechanical properties of samples extruded at 200 °C were examined and are given in Table 21.

Table 20 Composition, density, CTE and microhardness of pure Mg and the composite [20]

Material	Alumina (vol.%)	Density (g/cm ³)	CTE (10 ⁻⁶ K ⁻¹)	Microhardness (HV)
Mg	–	1.754 ± 0.009	29.4 ± 0.7	39.6 ± 2.1
Mg1Al ₂ O ₃	0.4	1.795 ± 0.010	28.1 ± 0.9	52.3 ± 1.1

Table 21 Thermal and mechanical properties of Mg/Al₂O₃ and pure Mg samples extruded at 200 °C [21]

Material	Al ₂ O ₃ (wt%)	CTE (10 ⁻⁶ K ⁻¹)	Hardness (HV)	0.2 YS (MPa)	UTS (MPa)	Elongation (%)
Mg (E200 °C)	–	30.6 ± 0.9	37.8 ± 0.9	133 ± 12	172 ± 21	2.68 ± 1.0
Mg1Al ₂ O ₃ (E200 °C)	1	28.9 ± 0.3	43.7 ± 1.5	125 ± 15	158 ± 19	1.78 ± 0.5
Mg3Al ₂ O ₃ (E200 °C)	3	26.9 ± 0.1	47.0 ± 3.4	118 ± 2	148 ± 8	1.68 ± 0.8
Mg5Al ₂ O ₃ (E200 °C)	5	22.0 ± 0.0	48.4 ± 3.8	103 ± 2	136 ± 5	1.63 ± 0.3
Mg (E400 °C, sint.)	–	29.4 ± 0.7	39.6 ± 2.1	148 ± 8	188 ± 7	1.75 ± 0.1
Mg1Al ₂ O ₃ (E400 °C, unsint.)	1	n.det.	44.8 ± 2.5	154 ± 11	200 ± 4	3.10 ± 0.7
Mg1Al ₂ O ₃ (E400 °C, sint.)	1	28.1 ± 0.9	52.3 ± 1.1	181 ± 4	226 ± 4	3.75 ± 1.2

The reduction in CTE due to the lower CTE of alumina and the increased hardness due to the high hardness of alumina were expected. The decrease of 0.2 YS, UTS and failure strain with increasing amounts of alumina nanoparticles is attributed to imperfect bonding at the interface and reduced cavitation resistance of the composite. In order to improve on these issues, a higher extrusion temperature and sintering steps were included in the production process. The material properties are shown in the lower part of Table 21. Sintering and extrusion at 400 °C increases the mechanical strength of pure magnesium, but also of the composite with 1 wt% alumina.

Magnesium alloy AZ31B was used as the matrix alloy for reinforcement with three different amounts of 50 nm size alumina [22]. 0.66, 1.11 and 1.5 vol.% reinforcement was introduced by the DMD process, where the superheated melt was stirred and subsequently released through two argon jets normal to the melt stream (see also [12]). The materials obtained were then hot extruded at 350 °C. Macrostructural investigations revealed no presence of macropores and shrinkage cavities or other macrostructural defects. The results of density measurements and grain size characterisation are listed in Tables 22 and 23. The small effect of particulate content on the grain size expresses the ineffectiveness of alumina nanoparticles in neither nucleating the solidification process nor being an obstacle for grain growth. The addition of alumina nanoparticles led to significant reductions in 0.2 YS and UTS. The amount of Al₂O₃ barely influences the reduction of these properties. The elongation to fracture is significantly increased by increasing the amount of alumina nanoparticles. Also the work of fracture increases, which can directly contribute to the higher elongation. The same materials were

investigated in [23] revealing their compressive response. Compressive properties are given in Table 24. 0.2 CYS, UCS and failure strain increases with an increasing amount of nanoparticles.

In a further study, the materials were investigated to determine their oxidation behaviour [24] using a DTA-TG setup. The materials were heated up with a ramping rate of 50 K/min and the kinetics of weight change were detected and compared with specimens heated up in air. It was found that with an increasing amount of alumina particles the oxidation tendency is reduced. At temperatures of 450 °C there is a change from parabolic to linear oxidation behaviour, which may be attributed to defects in the oxide layer. Oxidation rates are given in Table 25.

Table 24 Compressive properties of AZ31B and AZ31B based composites [23]

Material	0.2 CYS (MPa)	UCS (MPa)	Failure strain (%)
AZ31B	133 ± 4	444 ± 10	12.6 ± 1.0
AZ31B0.66Al ₂ O ₃	172 ± 17	468 ± 10	13.4 ± 1.8
AZ31B1.11Al ₂ O ₃	174 ± 2	478 ± 11	13.5 ± 0.8
AZ31B1.5Al ₂ O ₃	176 ± 7	486 ± 5	14.3 ± 1.2

Table 25 Oxidation rates of AZ31B and the composites [24]

Material	Oxidation rate (mpy) at temperature				
	300 °C	350 °C	400 °C	450 °C	470 °C
AZ31B	51.9	74.6	89.2	165.5	394.9
AZ31B0.66Al ₂ O ₃	25.7	43.3	67.5	138.2	375.7
AZ31B1.11Al ₂ O ₃	13.6	27.7	50.3	117.2	307.7
AZ31B1.5Al ₂ O ₃	10.4	18.2	39.6	109.0	298.5

Table 22 Density, porosity and grain size of AZ31B and AZ31B based composites [22]

Material	Alumina content (vol.%)	Density (g/cm ³)		Porosity (%)	Grain size (µm)
		Theor.	Exp.		
AZ31B	–	1.77	1.77	0	5.8 ± 0.4
AZ31B0.66Al ₂ O ₃	0.66	1.7845	1.7841 ± 0.0037	0.06	4.5 ± 0.3
AZ31B1.11Al ₂ O ₃	1.11	1.7943	1.7933 ± 0.0026	0.06	3.9 ± 0.1
AZ31B1.5Al ₂ O ₃	1.5	1.8098	1.8086 ± 0.0028	0.07	3.1 ± 0.03

Table 23 CTE, hardness and room temperature tensile properties of AZ31B and AZ31B based composites [22]

Material	CTE (10 ⁻⁶ K ⁻¹)	Micro-hardness (HV)	0.2 YS (MPa)	UTS (MPa)	Failure strain (%)	Work of fracture (J/m ³)
AZ31B	26.23	63 ± 1	201 ± 7	270 ± 6	5.6 ± 1.4	15 ± 3
AZ31B0.66Al ₂ O ₃	25.96	79 ± 4	149 ± 7	215 ± 15	14.6 ± 1.1	31 ± 4
AZ31B1.11Al ₂ O ₃	25.12	82 ± 2	148 ± 11	214 ± 16	25.5 ± 2.2	52 ± 2
AZ31B1.5Al ₂ O ₃	24.73	86 ± 3	144 ± 9	214 ± 16	29.5 ± 1.9	60 ± 3

The material produced using the DMD process described in [12] was investigated to determine its high-temperature strength [25]. An experimentally evaluated 0.2 Yield Strength was compared with a mathematical model for nanocomposites proposed by Zhang and Chen [26]. At RT and 150 °C the measured values are in good agreement with the model. At 200 °C the measured values decrease significantly compared to the model as can be seen in Fig. 2. The ductility increases significantly with increasing temperature.

AZ31 magnesium alloy was reinforced with 1.5 vol.% 50 nm alumina particles [27]. Two different arrangements of alloy pieces and particles during melting were performed, in order to vary the contact time between melt and reinforcement. The first material had a stirring time of 2.5 min and the second one of 5 min. After casting, the billets were machined and an extrusion of these billets at 350 °C was done. An investigation of microstructure and mechanical properties showed a dense material, without macropores and shrinkage cavities. The differences in

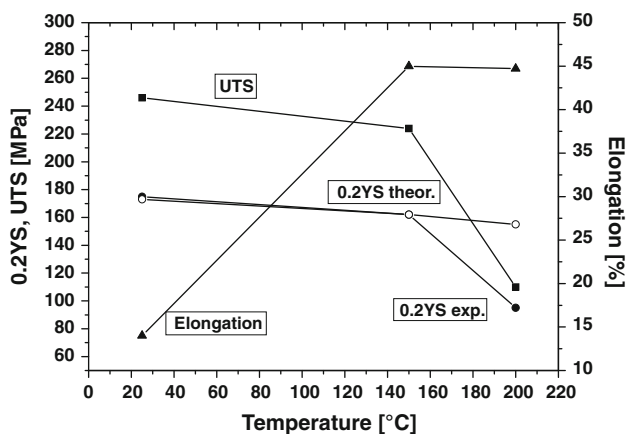


Fig. 2 Experimental mechanical properties and modelled 0.2 YS of the nanocomposite (after [25])

tensile strength are attributed to different textures in the longitudinal direction, in comparison with the second nanocomposite (Tables 26, 27).

Pure magnesium and AZ31 were reinforced with 0.5, 1 and 2 wt% alumina nanoparticles of 100 nm size [28]. An Mg 8 wt% master alloy was added to the alloys to obtain the composite materials. Small parts of the castings were hot rolled and subsequently annealed for recrystallization. Figure 3 shows the microstructures of the pure magnesium and the composites.

Measurement of the grain sizes of the castings and wrought materials show that there is a decrease in grain size with an increasing content of alumina nanoparticles (Fig. 4). This is due to heterogeneous nucleation sites during solidification in the case of castings and due to a pinning effect during recrystallization in the wrought case. CTE is slightly reduced with an increasing amount of alumina particles. Pure magnesium has a CTE of $27.9 \times 10^{-6} \text{ K}^{-1}$ and with 2 wt% alumina particles it is reduced to $25.9 \times 10^{-6} \text{ K}^{-1}$. AZ31 has a thermal expansion coefficient of $26.4 \times 10^{-6} \text{ K}^{-1}$ and with 2 wt% alumina particles it decreased to $25.2 \times 10^{-6} \text{ K}^{-1}$. This reduction is attributed to the low CTE of alumina ($7.4 \times 10^{-6} \text{ K}^{-1}$). Hardness increases with an increasing alumina content (Fig. 5). This is attributed to grain refinement and particle strengthening. The same behaviour can be seen in the tensile strength: 0.2 yield strength and the ultimate tensile strength increases while ductility decreases with increasing alumina content (Figs. 6, 7).

For evaluation of the hot-working behaviour of pure magnesium reinforced with 1 vol.% nano-alumina powder compared with unreinforced magnesium prepared the same way, a PM route was chosen to prepare the materials [29]. Magnesium powder with a size of 60–300 μm was mixed with alumina powder of 50 nm in a mechanical alloying machine for 1 h. The blend was subsequently cold compacted to billets and then sintered in a microwave sintering

Table 26 Grain characteristic, hardness and mechanical properties of AZ31 and the nanocomposite [27]

Material	Grain size (μm)	Microhardness (HV)	0.2 YS (MPa)	UTS (MPa)	Elongation (%)	WOF (MJ/m^3)
AZ31	4.0 ± 0.9	64 ± 4	172 ± 15	263 ± 12	10.4 ± 3.9	26 ± 9
AZ31/1.5Al ₂ O ₃ -2.5	2.3 ± 0.7	83 ± 5	204 ± 8	317 ± 5	22.2 ± 2.4	68 ± 7
AZ31/1.5Al ₂ O ₃ -5	3.1 ± 0.0	86 ± 3	144 ± 9	214 ± 16	19.5 ± 1.9	60 ± 3

Table 27 Mechanical properties of compressive testing of AZ31 and the nanocomposite [27]

Material	0.2 CYS (MPa)	UCS (MPa)	Ductility (%)	WOF (MJ/m^3)
AZ31	93 ± 9	486 ± 4	19.7 ± 7.2	76 ± 14
AZ31/1.5Al ₂ O ₃ -2.5	98 ± 2	509 ± 12	19.0 ± 2.7	84 ± 15
AZ31/1.5Al ₂ O ₃ -5	113 ± 8	531 ± 14	24.2 ± 1.0	112 ± 11

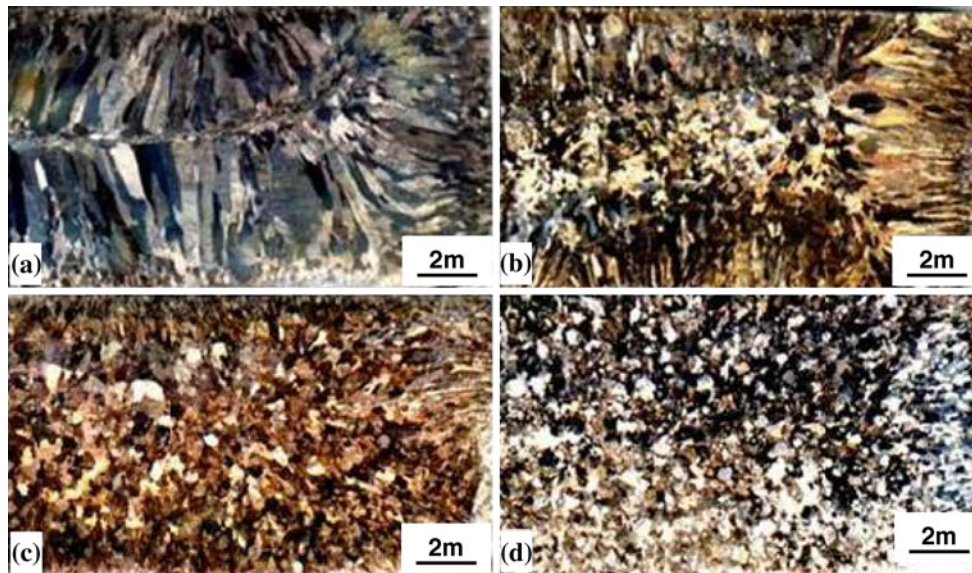


Fig. 3 Macro-etched cross-sections of the as-cast samples: **a** Mg, **b** Mg-0.5Al₂O₃, **c** Mg-1Al₂O₃ and **d** Mg-2Al₂O₃ [28] (with friendly permission of R. Mahmudi)

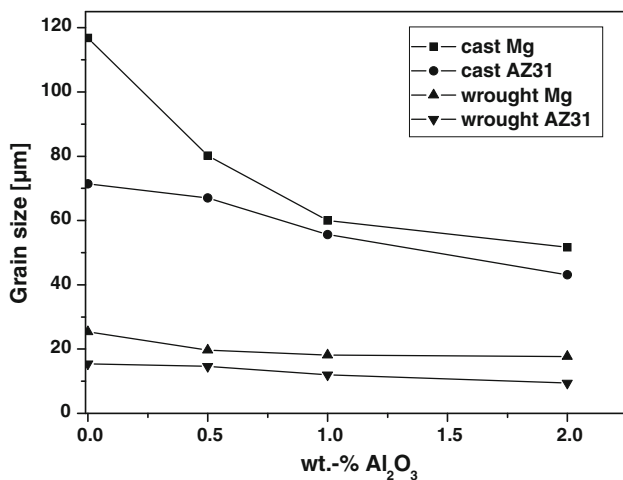


Fig. 4 Grain size of Mg and AZ31 as a function of alumina content [28] (with friendly permission of R. Mahmudi)

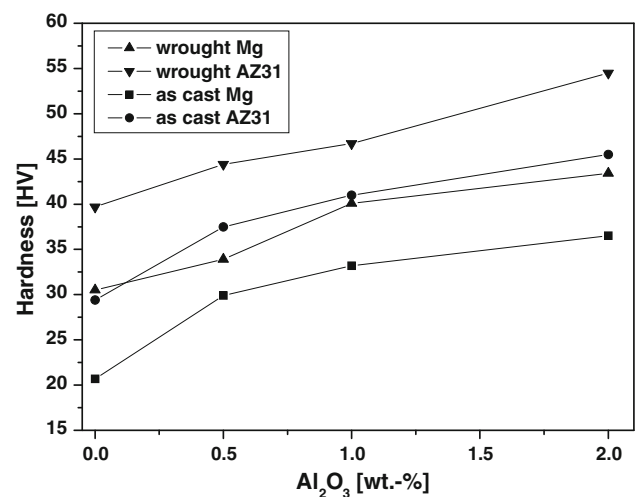


Fig. 5 Hardness of Mg and AZ31 and its composites dependant on alumina content [28] (with friendly permission of R. Mahmudi)

process. After soaking at 400 °C for 1 h, the materials were hot extruded at 350 °C. For configuration of deformation maps, uniaxial compression tests with deformation rates between 0.0003 and 10 s⁻¹ and temperatures between 300 and 500 °C were performed. Optical investigations have shown that alumina nanoparticles are not present within the magnesium particles, but decorate the former boundaries. As can be seen in Fig. 8, the composite material always exhibits higher flow stress compared to the pure magnesium at 300 and 450 °C, respectively. The difference increases with decreasing strain rate. The nanoparticle reinforcement seems to enhance the high temperature strength, especially at low strain rates.

The processing map made from the compression tests shows different areas of hot deformation properties (Fig. 9). In the temperature range between 300 and 500 °C and at strain rates between 0.1 and 10 s⁻¹ there is a domain with optimum workability. This domain shows its maximum at 420 °C and 10 s⁻¹ strain rate. An instable regime can be found in the temperature range between 400 and 500 °C at low strain rates below 0.01 s⁻¹. In this regime, hot working is not expected to be favourable. In the processing map of pure magnesium at the same conditions, three deformed domains have been identified. The first regime between 400 and 500 °C with strain rates between 0.001 and 1 s⁻¹ represents dynamic recrystallization, in the

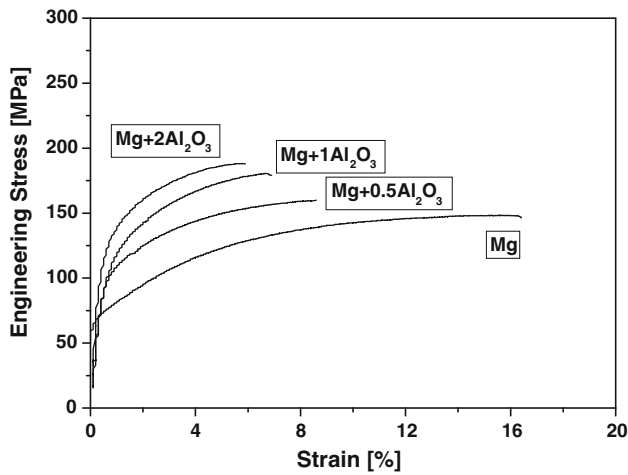


Fig. 6 Stress–strain curves of wrought magnesium-based materials [28] (with friendly permission of R. Mahmudi)

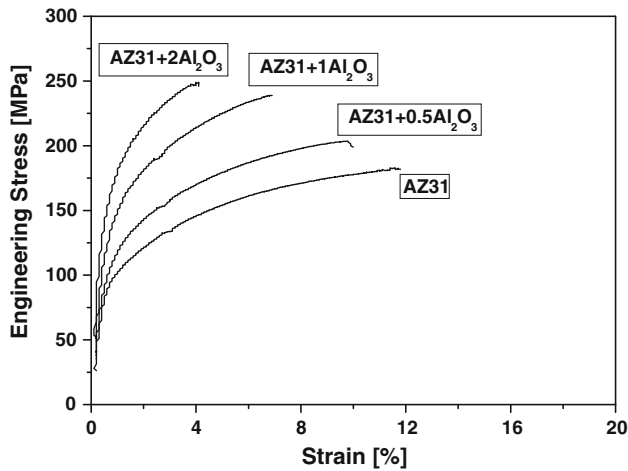


Fig. 7 Stress–strain curves of wrought AZ31-based materials [28] (with friendly permission of R. Mahmudi)

same way as the second domain in the area between 320 and 440 °C with strain rates between 1 and 10 s⁻¹. The third domain between 470 and 500 °C with strain rates between 1 and 10 s⁻¹ is expected to represent inter-crystalline cracking.

To describe the kinetics of hot deformation depending on the strain rate and temperature, the variation of log flow stress with log strain rate in the first case and the variation of log flow stress with T^{-1} has to be plotted. The pure magnesium shows constant linear stress exponents of 5.0 at 450 °C and 6.06 at 350 °C. The composite material at both temperatures shows a non-linear behaviour with a deviation in the region of 0.1 s⁻¹. Below 0.1 s⁻¹, the stress exponent is approximately 15.4 and at higher strain rates it is 6.25. The Arrhenius plots at strain rates of 0.1 and 10 s⁻¹, respectively, give apparent activation energies of approximately 123 kJ/mol for the composite and the matrix

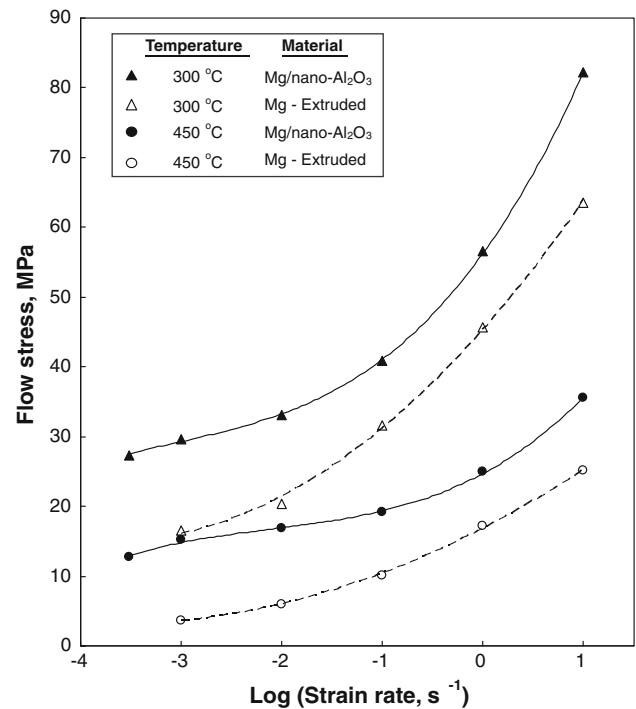


Fig. 8 Variation of flow stress at a true strain rate of 0.5 with logarithm of strain rate at 300 and 450 °C for the composite and pure magnesium [29] (with friendly permission of K. P. Rao)

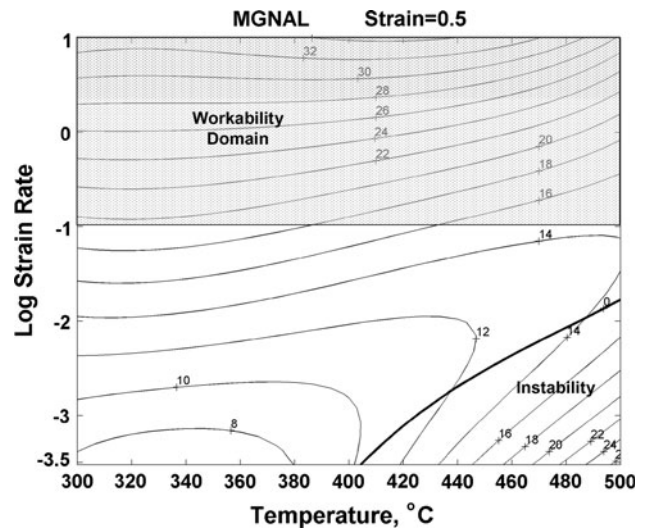


Fig. 9 Processing map of the composite material at a strain of 0.5 [29] (with friendly permission of K.P. Rao)

as well. At lower strain rates the composite exhibits high apparent activation energy of 305 kJ/mol and the unreinforced magnesium approximately 136 kJ/mol, which is close to the activation energy for self-diffusion (135 kJ/mol). A significant reduction of self-diffusion in the composite is suggested, which may be responsible for the increased strength at low stresses. Optical metallography of the microstructure after deformation reveals that the former

boundaries of the magnesium particles, which are decorated with the nanoparticles are stable during hot deformation. They do not rotate or slide against each other.

SiO₂

Magnesium alloy AZ61 was reinforced with SiO₂ particles with a size of 20 nm using a friction stir process (FSP) [30]. A groove was cut into a magnesium alloy bar and the nano-powder was filled into the groove. In order to close the cut, a flat FSP tool was used, followed by a normal pin and shoulder tool for mixing the reinforcement into the alloy. Two material samples were produced; containing 5 and 10 vol.% SiO₂, respectively. The size of SiO₂ decreases with tool passes stirring the same area. The silica cluster size and average grain size are given in Table 28. The grain size in an unreinforced AZ61 billet was 75 μm and after 4P FSP 7–8 μm.

The mechanical properties of AZ61 and the composites produced using FSP are given in Table 29. An increase in

hardness and strength of the unreinforced AZ61 after FSP can be attributed to grain refinement during processing. An improvement of strength with a reduction of ductility is achieved by the reinforcement of silica. Tensile tests at 350 °C yielded elongation of 350% at 10⁻² s⁻¹ and 420% at 10⁻¹ s⁻¹, which clearly exhibits a high strain-rate superplasticity.

Y₂O₃

The liquid metal infiltration of a ceramic perform, consisting of 30 vol.% of 280 nm yttria particles, was carried out for processing magnesium composites reinforced with nano-yttria. As-cast billets were hot extruded with an extrusion ratio of 20 at a temperature of 400 °C. Microstructural characterisation and mechanical properties [31] as well as creep behaviour [32] was investigated. The density of extruded Mg/30Y₂O₃ was 2.7154 ± 0.0024 g/cm³ and, assuming no porosity and the densities of magnesium and yttria to be 1.74 and 5.03 g/cm³ respectively, a volume fraction of 29.7 ± 0.001% was estimated. Elastic properties were measured by ultrasonic techniques and the results are given in Table 30. The measured values are in good agreement with prediction by the Eshelby model. The compressive strength is quite high and Orowan strengthening as well as Hall–Petch strengthening is assumed to be responsible.

In [32], the creep behaviour was determined at temperatures between 200 and 450 °C and stresses between 7 and 125 MPa. A compressive creep with constant load was performed and the true stress was calculated at the deformation where the minimum creep rate was achieved. Double logarithmic plots of minimum creep rate and true

Table 28 SiO₂ cluster size and grain size in composites with 5 vol.% (1D) and 10 vol.% (2D) silica after 1, 2, 3 and 4 tool passes (1P, 2P, 3P and 4P) [30]

	1D1P	1D2P	1D3P	1D4P
SiO ₂ cluster size (nm)	600	210	210	190
Average grain size (μm)	3.1	2.8	2.0	1.8
	2D1P	2D2P	2D3P	2D4P
SiO ₂ cluster size (nm)	300	200	170	150
Average grain size (μm)	1.5	1.5	1.0	0.8

Table 29 Mechanical properties of AZ61 and the composites at room temperature [30]

Material	Hardness (HV)	Yield strength (MPa)	UTS (MPa)	Elongation (%)
AZ61 billet	60	140	190	13
AZ61 after 4P FSP	72	147	242	11
1D2P (5 vol.%, 2 passes)	91	185	219	10
1D4P (5 vol.%, 4 passes)	97	214	233	8
2D2P (10 vol.%, 2 passes)	94	200	246	4
2D4P (10 vol.%, 4 passes)	105	225	251	4

Table 30 Elastic properties of extruded Mg/30Y₂O₃ and predictions by models and compression yield strength, ultimate strength and deformation [31]

Mg/30Y ₂ O ₃	G (GPa)	ν	E (GPa)	E _(Shear-lag) (GPa)	E _(Eshelby) (GPa)	σ _{0.2} (MPa)	UCS (MPa)	A (%)
Longit.	23.0	0.30	59.8	49.8	64.4	344	455	>20
Transv.	25.0	0.27	63.6	49.8	64.4			

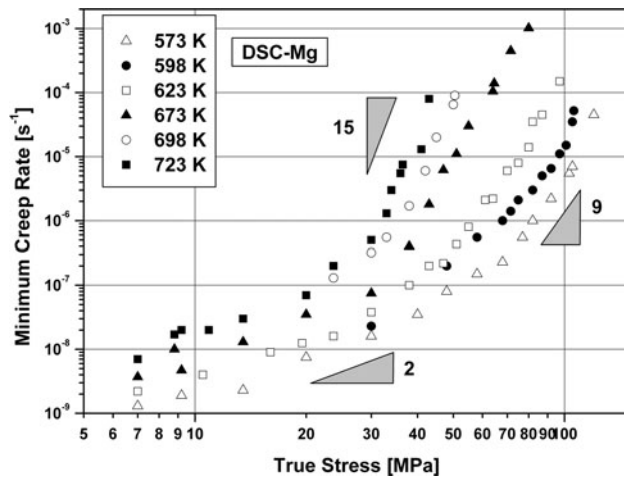


Fig. 10 Double logarithmic plot of minimum creep rate and stress for yttria reinforced magnesium [32] (with friendly permission of D.C. Dunand)

stress (Fig. 10) give the apparent stress exponent n_{app} in accordance with the power law constitutive creep equation 4:

$$\dot{\epsilon}_s = K \sigma^{n_{app}} \exp\left(-\frac{Q_{app}}{RT}\right) \quad (4)$$

where $\dot{\epsilon}_s$ is the minimum creep rate, K a material dependent constant, Q_{app} the apparent activation energy for creep, T the absolute temperature and R the gas constant. Two distinct areas exist above and below approximately 35 MPa: constant values for $n_{app} = 2$ below 35 MPa and between 9 and 15 for above 35 MPa can be estimated. For diffusion or dislocation controlled creep, expected n -values are 1 and 5, respectively.

The apparent activation energy for creep, Q_{app} , can be estimated by plots of $\ln \dot{\epsilon}_s$ over $1/T$ and shows the calculated values for different stresses. At low stresses Q_{app} is about half the value of activation energy for grain boundary diffusion in pure magnesium ($Q_{gb} = 92$ kJ/mol). In the high stress regime, the apparent activation energy increases to a maximum value of 325 kJ/mol, which is much more than the activation energy for lattice diffusion in pure magnesium ($Q_l = 135$ kJ/mol). Figure 11 shows this increasing trend in apparent activation energy. In calculating a threshold stress, it was found that the values are close to predictions by a general climb model at low temperatures. At higher temperatures it reaches only about 60% of the predicted values.

Pure magnesium powder in combination with yttria particles of two different sizes were used for a study of the tension/compression anisotropy behaviour of the resulting composites [33]. In a PM route, magnesium powder (45 μm) and two different sizes of yttria powder (6 μm and

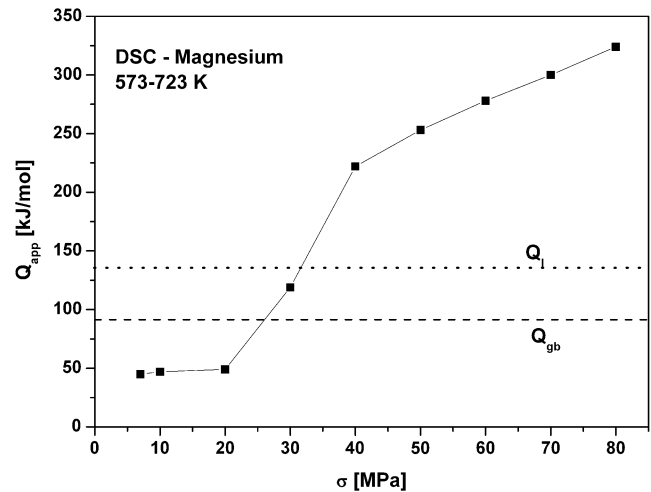


Fig. 11 Apparent activation energy for creep as a function of stress in yttria reinforced magnesium [32] (with friendly permission of D.C. Dunand)

<1 μm) were mixed. 5, 10, 15 and 20 vol.% particles were added, blended and subsequently cold compacted, followed by hot extrusion at 400 $^{\circ}\text{C}$ with an extrusion ratio of 18. The texture of the extruded composites was studied and compared with the texture of extruded pure magnesium. The texture is similar in all materials, but the intensity decreases with an increasing amount of yttria. Particle stimulated nucleation (PSN) is suggested to be responsible. Hardness and Young's modulus increase with an increasing amount of ceramic particles. A strong asymmetry of yield strength in tension and compression is seen in the case of unreinforced magnesium. Yield stress is higher in tension. With an increasing amount of yttria particles, the difference between tension and compression yield stress decreases and equals approximately 15 vol.%. With higher amounts of yttria it is even higher in compression.

A DMD technique was used to produce yttria-reinforced (average size: 29 nm) pure magnesium, with three different concentrations of reinforcement [34] (Table 31). Hot extrusion was performed as a second processing step. Hardness, tensile strength and yield stress increases with an increasing amount of yttria particles up to a content of 0.66 vol.%. The composite with a higher content (1.11 vol.%) shows a decreasing hardness, strength and ductility (Table 32). A change to inter-granular fracture as the predominant mode seems to be responsible for this effect.

Magnesium powder of 98.5% purity and yttria nanopowder with a particle size between 30 and 50 nm were used to produce two composites with yttria concentrations of 0.5 and 2.0 wt%, respectively [35]. The powders were blended for 1 h and compacted to billets with a pressure of 97 bar. After a microwave sintering process, the billets

Table 31 Density, porosity and grain size of yttria reinforced magnesium [34]

Material	Yttria content (wt%)	Density (g/cm ³)		Porosity (%)	Grain size (μm)
		Theor.	Exp.		
Mg/0.00Y ₂ O ₃	–	1.74	1.7397 ± 0.0009	0.02	49 ± 8
Mg/0.22Y ₂ O ₃	0.6	1.7472	1.7472 ± 0.0029	0.00	10 ± 1
Mg/0.66Y ₂ O ₃	1.9	1.7616	1.7598 ± 0.0015	0.10	6 ± 1
Mg/1.11Y ₂ O ₃	3.1	1.7763	1.7730 ± 0.0036	0.19	6 ± 2

Table 32 Mechanical properties of yttria reinforced magnesium [34]

Material	Hardness		0.2 YS (MPa)	UTS (MPa)	Ductility (%)	Work of fracture (J/m ³)
	Macro (15 HRT)	Micro (HV)				
Mg/0.00Y ₂ O ₃	37 ± 1	40 ± 0	97 ± 2	173 ± 1	7.4 ± 0.2	11.1 ± 0.3
Mg/0.22Y ₂ O ₃	56 ± 1	51 ± 0	218 ± 2	277 ± 5	12.7 ± 1.3	29.6 ± 3.5
Mg/0.66Y ₂ O ₃	58 ± 0	56 ± 0	312 ± 4	318 ± 2	6.9 ± 1.6	18.2 ± 4.7
Mg/1.11Y ₂ O ₃	49 ± 0	52 ± 1	–	205 ± 3	1.7 ± 0.5	1.9 ± 0.7

were hot extruded at a temperature of 350 °C. For the purposes of comparison, pure magnesium was also processed. A microstructural characterisation was performed and the results are given in Table 33. Mechanical tests and thermal expansion measurements were performed and the results are given in Table 34.

The reduction of CTE can be attributed to the low CTE of yttria ($7.6 \times 10^{-6} \text{ K}^{-1}$) and a good bonding between particles and the matrix. With an increasing amount of yttria 0.2 YS, UTS and ductility also increases. The ductility increase is attributed to activation of non-basal slip systems and the tendency of yttria nanoparticles to enhance cross-slip of dislocations. The same materials were investigated to determine the extrusion ratio and its influence on

the mechanical properties [36]. Pure magnesium and 2 wt% nano-yttria reinforced magnesium was extruded with ratios of 12:1, 19:1 and 25:1, respectively. With increasing ratios the density increases, due to a decrease in porosity. The microhardness tests revealed an increase in hardness with increasing ratio. This is attributed to an improvement in yttria distribution, decreasing grain size and reduction of porosity. Both materials show an increase in yield strength and ultimate strength with increasing extrusion ratio. Both effects are also attributed to the grain size reduction and the decrease of porosity.

Turnings of pure magnesium and yttria particles with a size between 32 and 36 nm were used to produce a composite material using the DMD technique and with the

Table 33 Density, porosity and grain size of yttria reinforced Mg [35]

Material	Yttria content (vol.%)	Density (g/cm ³)	Porosity (%)	Grain size (μm)
Mg	–	1.74 ± 0.01	0.13	20 ± 3
Mg/0.5Y ₂ O ₃	0.17	1.73 ± 0.01	0.87	19 ± 3
Mg/2.0Y ₂ O ₃	0.7	1.76 ± 0.01	0.35	18 ± 3

Table 34 Mechanical properties and CTE of yttria reinforced Mg [35]

Material	0.2 YS (MPa)	UTS (MPa)	Ductility (%)	Work of fracture (MJ/m ³)	CTE (10 ⁻⁶ K ⁻¹)	Microhardness (HV)
Mg	134 ± 7	193 ± 1	7.5 ± 2.5	12.9 ± 4.8	28.2 ± 0.0	37 ± 2.0
Mg/0.5Y ₂ O ₃	144 ± 2	214 ± 4	8.0 ± 2.8	16.6 ± 4.2	21.3 ± 0.1	38 ± 0.4
Mg/2.0Y ₂ O ₃	157 ± 10	244 ± 1	8.6 ± 1.2	21.8 ± 3.1	20.8 ± 0.6	45 ± 2.0

Table 35 Morphology, density, mechanical properties and CTE of magnesium and yttria containing composites [37]

Material (+vol.%)	Grain size (μm)	Density (g/cm^3)	0.2 YS (MPa)	UTS (MPa)	Ductility (%)	CTE (10^{-6}K^{-1})
Mg	15.9 ± 3.8	1.738 ± 0.010	126 ± 7	192 ± 5	8.0 ± 1.6	28.73 ± 0.59
Mg/0.5Y ₂ O ₃	16.2 ± 3.6	1.742 ± 0.008	141 ± 1	223 ± 5	8.5 ± 1.6	27.81 ± 0.36
Mg/1.0Y ₂ O ₃	12.2 ± 4.0	1.743 ± 0.002	151 ± 5	222 ± 4	6.8 ± 0.5	27.02 ± 0.75
Mg/2.0Y ₂ O ₃	11.5 ± 3.2	1.749 ± 0.003	162 ± 10	227 ± 11	7.0 ± 0.5	26.82 ± 0.46

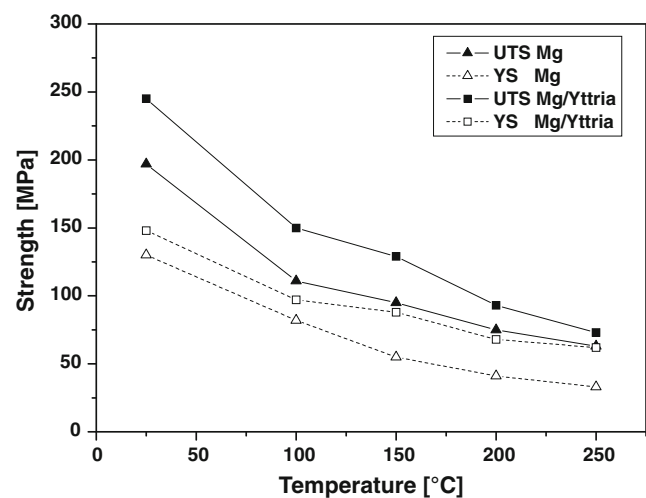
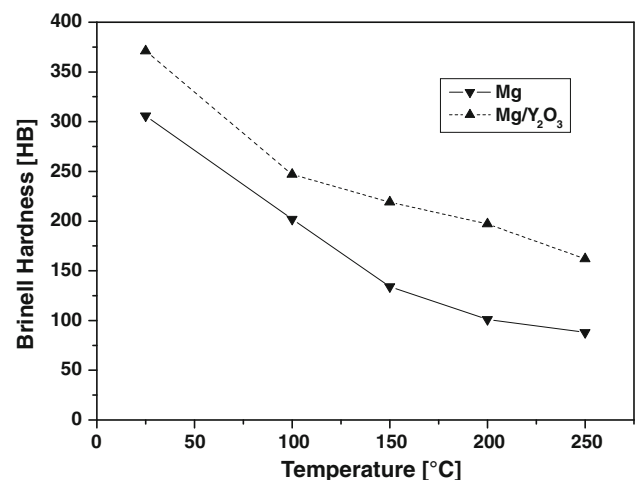
unreinforced material as well [37]. The ingots obtained were turned and then hot extruded at 350 °C. The smaller grain size with increasing yttria concentration is attributed to grain boundary pinning, which prevents grain growth during extrusion (Table 35).

Orowan strengthening and dislocation generation due to the large CTE mismatch between yttria particles and the magnesium matrix are attributed to be the main contributing factors for the increase in yield strength. In another study the same materials were fatigue tested [38]. It was found that with an increasing amount of yttria nanoparticles the fatigue life of a specimen increases and hardening during fatigue is attributed to the interaction between the particles and dislocations.

For the evaluation of high-temperature strength and hardness, pure magnesium powder with a size of 60–300 μm was blended for 1 h with 2 wt% yttria powder with a size of 30–50 nm [39]. The mixture was subsequently cold compacted under a pressure of 97 bar and the resulting cylindrical billets were sintered at 640 °C. The sintered billets were hot extruded at 350 °C with an extrusion ratio of 25. Pure magnesium rods were prepared the same way for comparison. Both materials were tested in terms of tensile strength and hardness at temperatures of 25, 100, 150, 200 and 250 °C. Metallographic investigation of the composite material shows a relatively good distribution of the nanoparticles and only a few clusters and nano-pores. The grain sizes of the pure magnesium and the composite are 20 ± 3 and $18 \pm 3 \mu\text{m}$, respectively, which is only an insignificant variation. XRD studies were performed with both materials in the ‘as produced’ state and after hot deformation at 250 °C. The absence of MgO peaks shows that there is no decomposition of Y₂O₃ during the processing or the high-temperature tensile testing. The significant reduction of the intensity of the (0002) peak in the composite, compared to the monolithic magnesium, is assumed to be due to the rotation of basal planes, preferentially in the [10-11] direction. The composite material would exhibit a stronger basal texture compared to the magnesium, which could be the reason for its higher yield strength (see Fig. 12). Basal slip is limited.

At all temperatures, the hardness measurements revealed a higher hardness in the composite material

compared to pure magnesium (see Fig. 13). With increasing test temperature, the hardness decreases in both cases. This is attributed to the softening effect of higher temperatures, due to thermal expansion.

**Fig. 12** Temperature dependence of UTS and YS of magnesium and the magnesium/yttria composite (after [39])**Fig. 13** Hardness variation with temperature in pure magnesium and in the yttria containing composite (after [39])

Carbon nanotubes (CNT)

In recent years, CNT or multi-walled carbon nanotubes (MWCNT) have become popular for reinforcing metals and even polymers. These nanotubes show extremely high mechanical properties and flexibility as well as a high Young’s modulus. Their small size reduces the possibility of thermal mismatch-induced dislocation generation at the matrix/tube interface, which is seen as a further advantage. MWCNTs were introduced into the surface of an AZ31 alloy by friction stir processing (FSP) to modify the surface [40]. The tubes have a length of 250 nm and an outer diameter of 20–50 nm and were combined with an AZ31 plate of 6 mm thickness. A groove was cut into the sheet and filled with nanotubes before the FSP was performed. It could be shown that the MWCNTs are dispersed randomly into the matrix. The best distribution was achieved at a speed of 25 mm/min and a rotation speed of 1500 r/min. Grain refinement was promoted in the reinforced areas. The hardness of maximum 78 HV is attributed to the nanotubes and to the grain refinement. Hardness of unreinforced AZ31 in the as-received state and after FSP state was 41 HV and 55 HV, respectively.

The DMD technique was used to produce composite material of pure magnesium reinforced with 0.3, 1.3, 1.6

and 2 wt% of carbon nanotubes [41]. The process has already been described. For the purposes of comparison, pure magnesium was processed in the same way. Following DMD, the ingots were hot extruded at 350 °C with an extrusion ratio of 20.25. A slight increase in hardness is measurable with low amounts of CNT (Table 36). The hardness drops from amounts of 1.3% and above. Yield, tensile strength and ductility show the highest values at 1.3 wt% CNT. The activation of further slip planes is attributed as responsible for this higher ductility.

A comparative study of CNT-reinforced magnesium produced using a PM and a liquid metallurgical (LM) technique is performed in [42]. For the liquid process, magnesium turnings of 99.9% purity and CNT with an average diameter of 20 nm were cast using the DMD technique and subsequently hot extruded at 350 °C. For the powder technique, magnesium powder was mixed with 0.3 wt% nanotubes for 10 h and compacted to billets. After sintering for 2 h, the billets were also hot extruded at a temperature of 350 °C. For comparison, both materials were processed without nanotubes, too. It can be seen in Table 37 that the reduction of CTE in the PM composite is more significant compared to the liquid processed. Yield and tensile strength of the PM processed composite is higher compared to the LM material. The authors attribute

Table 36 Density, macrohardness and mechanical properties of CNT reinforced magnesium [41]

Material	CNT (wt%)	Density (g/cm ³)	Macrohardness (HR15T)	0.2 YS (MPa)	UTS (MPa)	Elongation (%)
Mg (99.9%)	–	1.738 ± 0.010	45 ± 1	126 ± 7	192 ± 5	8.0 ± 1.6
Mg–0.3 wt% CNT	0.3	1.731 ± 0.005	48 ± 1	128 ± 6	194 ± 9	12.7 ± 2.0
Mg–1.3 wt% CNT	1.3	1.730 ± 0.009	46 ± 1	140 ± 2	210 ± 4	13.5 ± 2.7
Mg–1.6 wt% CNT	1.6	1.731 ± 0.003	42 ± 1	121 ± 5	200 ± 3	12.2 ± 1.7
Mg–2.0 wt% CNT	2.0	1.728 ± 0.001	39 ± 1	122 ± 7	198 ± 8	7.7 ± 1.0

Table 37 Density, CTE and mechanical properties of liquid (LM) and powder metallurgical (PM) processed nanocomposites [42]

Material	Density (g/cm ³)	CTE (10 ^{−6} K ^{−1})	0.2 YS (MPa)	UTS (MPa)	Elongation (%)
Mg (99.5%) LM	1.738 ± 0.010	28.73 ± 0.59	126 ± 7	192 ± 5	8.0 ± 1.6
Mg–0.25 wt% CNT LM	1.731 ± 0.005	27.82 ± 0.22	128 ± 6	194 ± 9	12.7 ± 2.0
Mg (98.5%) PM	1.738 ± 0.001	28.56 ± 0.28	127 ± 5	205 ± 4	9.0 ± 2.0
Mg–0.3 wt% CNT PM	1.736 ± 0.001	25.90 ± 0.93	146 ± 5	210 ± 6	8.0 ± 1.0

Table 38 Density, Young’s modulus and mechanical properties of MWCNT-reinforced magnesium alloy AZ91 [43]

Material	Density (g/cm ³)	E (GPa)	0.2 YS (MPa)	UTS (MPa)	Elongation (%)
AZ91D	1.80 ± 0.007	40 ± 2	232 ± 6	315 ± 5	14 ± 3
AZ91D–0.5CNT	1.82 ± 0.008	43 ± 3	281 ± 6	383 ± 7	6 ± 2
AZ91D–1CNT	1.83 ± 0.006	49 ± 3	295 ± 5	388 ± 11	5 ± 2
AZ91D–3CNT	1.84 ± 0.005	51 ± 3	284 ± 6	361 ± 9	3 ± 2
AZ91D–5CNT	1.86 ± 0.003	51 ± 4	277 ± 4	307 ± 10	1 ± 0.5

this result to the higher amount of MgO in the original material for the powder route, which was found in XRD analysis. Additional MgO is assumed to give a further strengthening effect to that of the CNT. In the case of the liquid processed composite, ductility was improved when compared to the unreinforced magnesium, whereas it is reduced slightly in the powder version.

Again a PM method was chosen to produce an AZ91-based CNT composite [43]. AZ91 powder with a diameter of 100 μm and MWCNT with a length of approx. 5 μm were physically blended and subsequently hot pressed. The amount of MWCNT in the composites is 0.5, 1, 3 and 5 wt%, respectively. The resulting material was hot extruded at 450 $^{\circ}\text{C}$ with an extrusion ratio of 9:1. Young's modulus and density increase with increasing amounts of nanotubes in the same way as the ductility reduces (Table 38). Yield and ultimate tensile strength show a maximum at an amount of approximately 1 wt% MWCNT addition.

References

- Regev M, Rosen A, Bamberger M (2001) *Metall Mater Trans* 32A:1335
- Clyne TW, Withers PJ (1993) *An introduction to metal matrix composites*. Cambridge University Press, Cambridge
- Zhang Q, Chen DL (2004) *Scripta Mater* 51:863
- Bata V, Pereloma EV (2004) *Acta Mater* 52:657
- Ferkel H, Mordike BL (2001) *Mater Sci Eng A* 298:193
- Ugandhar S, Gupta M, Sinha SK (2006) *Solid State Phenom* 111:79
- Wong WLE, Gupta M (2006) *Solid State Phenom* 111:91
- Lan J, Yang Y, Li X (2004) *Mater Sci Eng A* 386:284
- Cao G, Konishi H, Li X (2008) *Mater Sci Eng A* 486:357
- Shiying L, Feipeng G, Qiongyuan Z, Wenzhen L (2009) *Mater Sci Forum* 618–619:433
- Trojanova Z, Lukac P, Ferkel H, Mordike BL, Riehemann W (1997) *Mater Sci Eng A* 234–236:798
- Hassan SF, Gupta M (2005) *Metall Mater Trans* 36A:2253
- Wong WLE, Karthik S, Gupta M (2005) *J Mater Sci* 40:3395. doi:10.1007/S10853-005-0419-z
- Hassan SF, Gupta M (2005) *J Metastable Nanocryst Mater* 23:151
- Hassan SF, Gupta M (2008) *J Alloys Compd* 457:244
- Hassan SF, Gupta M (2006) *Mater Sci Eng A* 425:22
- Hassan SF, Gupta M (2006) *Compos Struct* 72:19
- Hassan SF, Gupta M (2006) *J Alloys Compd* 419:84
- Hassan SF, Gupta M (2005) *Mater Sci Eng A* 392:163
- Srikanth N, Zhong XL, Gupta M (2005) *Mater Lett* 59:3851
- Zhong XL, Gupta M (2005) *J Metastable Nanocryst Mater* 23:171
- Nguyen QB, Gupta M (2008) *J Alloys Compd* 459:244
- Nguyen QB, Gupta M (2008) *Compos Sci Technol* 68:2185
- Nguyen QB, Gupta M, Srivatsan TS (2009) *Mater Sci Eng* 500:233
- Hassan SF, Tan MJ, Gupta M (2008) *Mater Sci Eng A* 486:56
- Zhang Z, Chen DL (2006) *Scripta Mater* 54:1321
- Paramsothy M, Hassan SF, Bau NQ, Srikanth N, Gupta M (2009) *Mater Sci Forum* 618–619:423
- Habibnejad-Korayem M, Mahmudi R, Poole WJ (2009) *Mater Sci Eng A* 519:198
- Prasad YVRK, Rao KP, Gupta M (2007) *Compos Sci Technol* 69:1070
- Lee CJ, Huang JC, Hsieh PJ (2006) *Scripta Mater* 54:1415
- Han BQ, Dunand DC (2000) *Mater Sci Eng A* 277:297
- Han BQ, Dunand DC (2001) *Mater Sci Eng A* 300:235
- Garces G, Rodriguez M, Perez P, Adeva P (2006) *Mater Sci Eng A* 419:357
- Hassan SF, Gupta M (2007) *J Alloys Compd* 429:176
- Tun KST, Gupta M (2007) *Compos Sci Technol* 67:2657
- Tun KS, Gupta M (2008) *J Mater Sci* 43:4503. doi:10.1007/s10853-008-2649-3
- Goh CS, Wei J, Lee LC, Gupta M (2007) *Acta Mater* 55:5115
- Goh CS, Wei J, Gupta M (2007) *Key Eng Mater* 345–346:267
- Mallik A, Tun KS, Vedantam S, Gupta M (2010) *J Mater Sci* 45:3058. doi:10.1007/s10853-010-4312-z
- Morisada Y, Fujii H, Nagaoka T, Fukusumi M (2006) *Mater Sci Eng A* 419:344
- Goh CS, Wei J, Lee LC, Gupta M (2006) *Mater Sci Eng A* 423:153
- Goh CS, Wie J, Lee LC, Gupta M (2006) *Solid State Phenom* 111:179
- Shimizu Y, Miki S, Soga T, Itoh I, Todoroki H, Hosono T, Sakaki K, Hayashi T, Kim YA, Endo M, Morimoto S, Koide A (2008) *Scripta Mater* 58:267